

Accurate prediction of the critical heat flux for pool boiling on the heater substrate

Fengxun Hai(海丰勋), Wei Zhu(祝薇), Xiaoyi Yang(杨晓奕), and Yuan Deng(邓元)

Citation: Chin. Phys. B, 2022, 31 (**6**): 064401. DOI: 10.1088/1674-1056/ac523c
Journal homepage: http://cpb.iphy.ac.cn; http://iopscience.iop.org/cpb

What follows is a list of articles you may be interested in

Thermal apoptosis analysis considering injection behavior optimization and mass diffusion during magnetic hyperthermia

Yun-Dong Tang(汤云东), Jian Zou(邹建), Rodolfo C C Flesch(鲁道夫 C C 弗莱施), Tao Jin(金涛), and Ming-Hua He(何明华)

Chin. Phys. B, 2022, 31 (**1**): 014401. DOI: 10.1088/1674-1056/ac0819

Lattice Boltzmann simulation on thermal performance of composite phase change material based on Voronoi models

Meng-Yue Guo(郭孟月), Qun Han(韩群), Xiang-Dong Liu(刘向东), and Bo Zhou(周博)

Chin. Phys. B, 2021, 30 (**10**): 104401. DOI: 10.1088/1674-1056/ac041d

Establishment and evaluation of a co-effect structure with thermal concentration-rotation function in transient regime

Yi-yi Li(李依依), Hao-chun Zhang(张昊春)

Chin. Phys. B, 2020, 29 (**8**): 084401. DOI: 10.1088/1674-1056/ab9437

Uniformity principle of temperature difference field in heat transfer optimization

Xue-Tao Cheng(程雪涛), Xin-Gang Liang(梁新刚)

Chin. Phys. B, 2019, 28 (**6**): 064402. DOI: 10.1088/1674-1056/28/6/064402

Prediction of heat transfer of nanofluid on critical heat flux based on fractal geometry

Xiao Bo-Qi

Chin. Phys. B, 2013, 22 (**1**): 014402. DOI: 10.1088/1674-1056/22/1/014402

Accurate prediction of the critical heat flux for pool boiling on the heater substrate

Fengxun Hai(海丰勋)[1], Wei Zhu(祝薇)[2,3,†], Xiaoyi Yang(杨晓奕)[1], and Yuan Deng(邓元)[2,4,‡]

[1] *School of Energy and Power Engineering, Beihang University, Beijing* 100083, *China*
[2] *Research Institute for Frontier Science, Beihang University, Beijing* 100083, *China*
[3] *Beijing Advanced Innovation Center for Biomedical Engineering, Beihang University, Beijing* 100083, *China*
[4] *Hangzhou Innovation Institute, Beihang University, Hangzhou* 310052, *China*

(Received 25 November 2021; revised manuscript received 25 January 2022; accepted manuscript online 7 February 2022)

While the influence of liquid qualities, surface morphology, and operating circumstances on critical heat flux (CHF) in pool boiling has been extensively studied, the effect of the heater substrate has not. Based on the force balance analysis, a theoretical model has been developed to accurately predict the CHF in pool boiling on a heater substrate. An analytical expression for the CHF of a heater substrate is obtained in terms of the surface thermophysical property. It is indicated that the ratio of thermal conductivity (k) to the product of density (ρ) and specific heat (c_p) is an essential substrate property that influences the CHF. By modifying the well-known force-balance-based CHF model (Kandlikar model), the thermal characteristics of the substrate are taken into consideration. The bias of predicted CHF values are within 5% compared with the experimental results.

Keywords: boiling heat transfer, kandlikar model, critical heat flux, heater substrate

PACS: 44.05.+e, 44.35.+c, 44.25.+f **DOI:** 10.1088/1674-1056/ac523c

1. Introduction

Thermal management of high-power electronics requires cooling strategies capable of dissipating high heat flux while maintaining the device at low operating temperatures.[1,2] However, the heat transfer system is limited by the critical heat flux (CHF), at which the boiling process transitions from nucleate boiling to film boiling, causing an abrupt increase in the heater surface temperature. One of the most important aspects of avoiding burnout is how to predict the critical heat flux as precisely as possible.[3–5]

Over the last eight decades, the mechanisms that are responsible for the CHF have been the topic of extensive research and discussion.[6–8] Bubble interference,[9] hydrodynamic instability,[10] macrolayer dryout,[11] hot/dry spot,[12,13] and interfacial lift-off[14] are five potential mechanisms for accurately predicting pool boiling CHF that have been reported in the literatures. The hypothesis of hydrodynamic instability proposed by Zuber,[15] which is the first theoretical and mechanical CHF model, has received the most attention among the five mechanisms. Indeed, the majority of published pool boiling CHF research attempts to improve the Zuber model's prediction capabilities by accounting for parametric variables that are not incorporated in the original model. Kandlikar[16] in particular presents a theoretical model based on force balancing that accounts for the near-field influence of wettability on the CHF of an upward-facing smooth inclined flat plate, as well as the far-field effect of hydrodynamic instability.

Thermal properties,[17,18] orientation,[19,20] heater size,[21] contact angle,[16] and surface roughness[22] all have an impact on CHF. Despite the fact that CHF is established as a hydrodynamic phenomenon, a lot of researches highlight the importance of surface properties. Several studies investigated heater thickness effects on CHF in pool boiling.[17,18,23] Non-hydrodynamic factors like the thermal properties and thickness of the heater have a major impact on the CHF of a surface. Several studies[17,24,25] investigated the influence of heater thickness and thermal properties of the heater material on CHF. To study the effect of the heater substrate thermal properties on CHF, Tachibana *et al.*[25] experimentally determined the CHF on thin, vertically oriented ribbon heaters in water. The CHF was seen to be proportional to the heat capacity, which is the product of heater thickness, density, and specific heat of the heater. As can be anticipated, CHF increases asymptotically with increasing thickness in pool boiling, until it reaches a limiting value beyond which the increasing heater size does not play a role. Heater material is also regarded to be an essential factor affecting HTC and CHF.[26–28] Westwater *et al.*[26] established the CHF correlation, which indicated that a high thermal effusivity helps to transport heat away from the local dry area, delaying the occurrence of CHF. Grigoriev *et al.*[28] investigated the heater material effect on the CHF by the experiments of liquid nitrogen boiling on different materials' surfaces and found that the CHF increased with the increase of thermal effusivity. However, the impact of the thermal properties of the heater material on determining the CHF over thick

†Corresponding author. E-mail: zhu_wei@buaa.edu.cn
‡Corresponding author. E-mail: dengyuan@buaa.edu.cn

© 2022 Chinese Physical Society and IOP Publishing Ltd

heater surfaces that are beyond the asymptotic thickness has not been fully explored.

In this paper, an analytical equation for the CHF of a heater substrate in terms of surface thermophysical characteristics is established. Pool boiling studies are carried out using distilled water to conduct pool boiling experiments on three different heater substrates (aluminum, brass, and copper). To establish the important characteristics that can best forecast CHF changes, the thermal conductivity of the tested material varies from 109 W/m·K to 398 W/m·K and the thermal mass ($\rho c_{\rm p}$) ranges from 2.4×10^3 kJ/m^3·K to 3.4×10^3 kJ/m^3·K. Finally, Kandlikar's CHF model is tweaked to account for the effect of the heater's thermal properties on CHF. The anticipated CHF agrees well with the experiment and the literature, with a maximum inaccuracy of 5%.

2. Experimental procedure and setup

2.1. Pool boiling setup/measurement

Figure 1 shows the main pool boiling arrangement in detail. During the trials, the distilled (DI) water reservoir is kept at saturation temperature in the liquid chamber.[29] As shown in Fig. 1(b), the test heater rod has the size of Φ10 mm (diameter) × 20 mm (height) and is fixed spirally on a cartridge heater inside which is a 600 W silicon nitride ceramic heater. To guarantee minimal heat loss, the test rod is put inside a teflon enclosure and an air gap. The cartridge heater is wrapped by the thick glass wool to make sure of one dimensional heat conduction vertically. An electrical resistance auxiliary heater immersed in water in the liquid chamber serves as the heat source to maintain the saturation condition of DI water in the chamber. The liquid chamber has a side length of 150 mm, a thickness of 5 mm and a height of 200 mm and is directly open to the ambient atmosphere. Three thermocouples (TJ36-CASS-020U-6, OMEGA Engineering Inc.) are inserted half way into the 1 mm diameter drilled holes on one side of the test heater rod at 3 mm apart and are 0.4 mm from the top surface to measure the temperature distribution in the test heater rod. The signals from these thermocouples are received using OpreX data acquisition systems (GP 10) and the data from the acquisition systems is then transferred to the computer, recorded and analyzed using the UnivViewer program. The temperatures measured at specific points as shown in Fig. 1(b) are used to calculate heat flux, wall superheat and heat transfer coefficient, which will determine the pool boiling efficiency.

The heat flux to the test surface is calculated based on one-dimensional heat transfer equation,[30] Fourier's Law:

$$q=-k_{\rm Cu}\frac{{\rm d}T}{{\rm d}x}, \tag{1}$$

where $k_{\rm Cu}$ is the thermal conductivity of copper, and ${\rm d}T/{\rm d}x$ denotes the temperature gradient along the heat flux, which is calculated using a three-point Taylor backward space series approximation from the thermocouples in the rod as follows:

$$\frac{{\rm d}T}{{\rm d}x}=\frac{3T_1-4T_2+T_3}{2\Delta x}, \tag{2}$$

where T_1, T_2, and T_3 are the temperatures along the test rod as shown in Fig. 1(b), and Δx means the distance between the adjacent thermocouples. The boiling surface temperature $T_{\rm wall}$ is calculated by one dimensional heat conduction equation by using the temperature measured inside the sample:

$$T_{\rm wall}=T_1-q\left(\frac{\Delta x_1}{k_{\rm Cu}}\right), \tag{3}$$

where Δx_1 denotes the distance between the boiling surface and thermocouple T_1. The boiling heat transfer coefficient (HTC) is calculated from measuring the heat flux and wall superheat, which is determined as follows:

$$h=\frac{q}{T_{\rm wall}-T_{\rm sat}}, \tag{4}$$

where $T_{\rm sat}$ denotes the saturated temperature of water inside the liquid chamber.

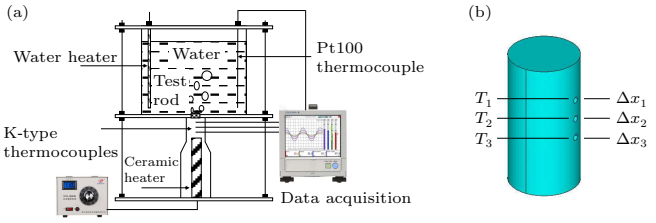


Fig. 1. (a) Schematic diagram of Pool boiling experimental setup; (b) the processed test sample rod which is screwed to the cartridge heater.

2.2. Uncertainty analysis

The main sources of uncertainty for the current setup were the bias and the precision errors. The bias error arises due to the calibration of the thermocouple, and the precision error is a result of the sensitivity of the measurement. For this study, uncertainty analysis is performed similar to that reported by Kandlikar and Patil.[31] The dimensional error due to sintering shrinkage, the limitation of the laser accuracy, and the solder layer thickness are ±0.01 mm; the temperature measurement uncertainty for the precise K-type thermocouples is ±0.2 K; and the power input uncertainty is ±1 W. The error propagation analysis revealed that the uncertainty of the observed heat transfer coefficient at CHF is about 7.8%, and the uncertainty of the heat flux is 2.5%, which is within the range of the literature.[32]

3. Result and discussion

The three selected substrates are made of copper, brass, and aluminum. All samples are treated with 7000 mesh sandpaper, which is one-way scratched sequentially from 1000 mesh to 2000 mesh, 5000 mesh, and 7000 mesh as

suggested.[33] To ensure repeatability, all samples are tested for three times.

Table 1 shows the thermal properties of the substrates tested. Each of the test heater rods is 20-mm high, and made of copper, brass, and aluminum, to guarantee that the CHF corresponding to each heater tested is independent of heater thickness. The microgeometry of a surface is one characteristic that is known to play a role in defining the CHF of a surface.[34,35] The test surface is cleaned with sandpaper to remove artifacts of the machining process such as burrs, pits, and grooves, ensuring that the microgeometry of the surface did not change amongst the multiple substrates examined. In order to ensure that the microgeometry of the surface does not vary between the different substrates tested, the surface roughness of all the substrates is maintained close to 0.05 μm (±0.01 μm) which represented the average arithmetic surface height (Ra).[36] The roughness range is low enough that no observable variation in CHF can be seen as a result of surface features. The thermal characteristics of the various substrates are summarized, as well as their contact angles, are shown in Table 1.

Table 1. Thermal properties of the substrates tested.

Material	Density (kg/m^3)	Specific heat (J/(kg·K))	Thermal conductivity (W/m·K)	Contact angle (°)
Aluminum	2700	896	201	72
Brass	8500	380	109	71
Copper	8933	385	398	71

After polishing with 7000-mesh ultra-fine sandpaper, the contact angles of the three substrates, copper, brass, and aluminum, are shown in Fig. 2. The contact angles of plain surfaces are all around 71°, which eliminates the impact of the surface on CHF performance. The bubble departure diameter is a critical parameter which governs the lateral coalescence of bubbles and the enhancement of capillary feeding of liquid.[37] According to the Fritz equation[38]

$$d_{\mathrm{Fz}} = 0.0208\beta \left[\frac{\sigma}{g\left(\rho_{\mathrm{L}} - \rho_{\mathrm{G}}\right)}\right]^{1/2}, \tag{5}$$

where β is the static contact angle in degree, σ is the surface tension force, g is the gravitational force, and ρ_{L} and ρ_{G} are the liquid and vapor densities, respectively. The calculated departure bubble diameter of three tested surfaces (brass, aluminum and copper) are 4.04 mm, 4.09 mm, and 4.04 mm, which is not much different.

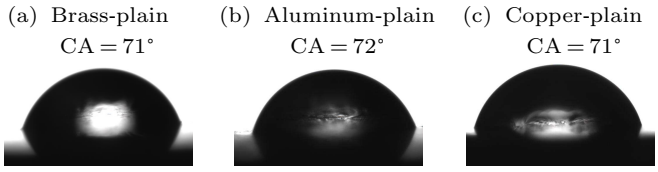


Fig. 2. Contact angles of plain surfaces of brass, aluminum, and copper.

The boiling heat transfer test apparatus is used to investigate and assess the performance of the three heat transfer substrates. Figure 3 shows the boiling curves of the three plain surfaces. As shown in Fig. 3(a), the CHF for aluminum is enhanced to 78.1 W/cm^2, which is approximately 1.56 times higher than that of the plain brass surface (50.1 W/cm^2). Moreover, the CHF for copper is 87.6 W/cm^2, which is approximately 1.75 times higher than that of the brass surface. As can be observed, the CHF varies depending on the heat transfer material, and the higher the heat conductivity, the higher the CHF value. Therefore a model is developed to calculate the impact of the physical properties of the material on the CHF.

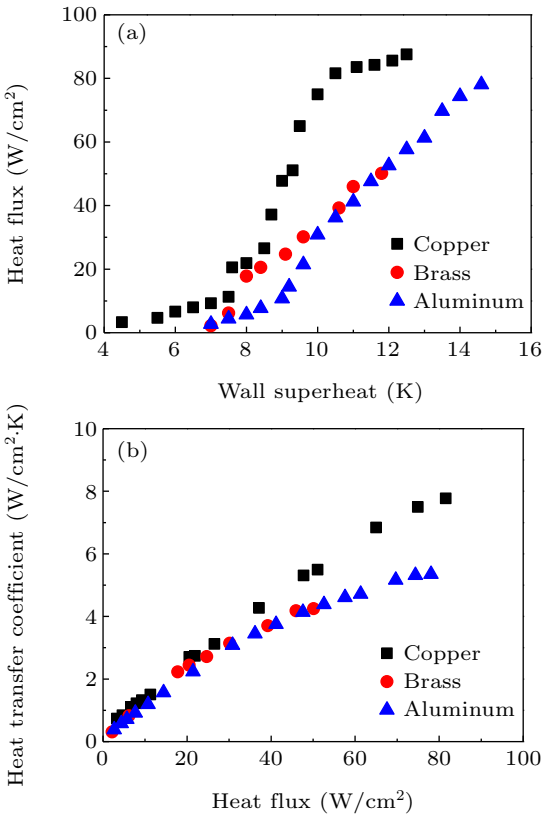


Fig. 3. (a) Pool boiling curves for the tested surfaces with water at atmospheric pressure. (b) Heat transfer coefficient comparison for the tested surfaces.

The heat transfer coefficient for the tested surfaces is shown in Fig. 3(b). When the critical heat flux on the plain copper surface is 87.6 W/cm^2, the heat transfer coefficient is 7.8 W/cm^2·K. The results reveal that surface materials have a substantial impact on CHF and HTC, with copper having the highest heat transfer coefficient and brass having the lowest one. At low heat flux, the difference is negligible, whereas

at high heat flux, copper outperforms aluminum by 47% and brass by 85%.

This variation in CHF is attributed to the heater surface's material properties, and further research in this study aims to improve the accuracy of CHF prediction by factoring in the impacts of heater material features. By considering the formation of steam jets above the nucleated bubbles and the liquid flow between the jets towards the heating surface, Kutateladze[39–41] proposed that the meaning of bubble generation and departure were lost near the critical heat flux condition, and critical condition is reached when the velocity in the vapor phase reaches a critical value. Following a dimensional analysis, he proposed the following correlation:

$$\frac{q}{h_{\mathrm{lv}}\rho_{\mathrm{v}}^{1/2}\left[\sigma g\left(\rho_{\mathrm{l}}-\rho_{\mathrm{v}}\right)\right]^{1/4}}=K, \tag{6}$$

where ρ_{v} is the density of bubbles, h_{lv} is the gas–liquid heat transfer coefficient, and ρ_{l} is the density of the liquid. The value of K was found to be 0.16 from the experimental data. Zuber[15] further formalized the concept of hydraulic instability and proposed a value of $K = 0.131$. According to this, the critical heat flux q of an ideal smooth surface is about 110 W/cm^2.

Kandlikar[16] proposed the Kandlikar model for predicting CHF while considering the impact of thermal performance. This model was modified by adding a dimensionless correction factor to Zuber's model, and the corresponding equations were given as

$$q = Kh_{\mathrm{lv}}\rho^{1/2}\left[\sigma g\left(\rho_{\mathrm{l}}-\rho_{\mathrm{v}}\right)\right]^{1/4}, \tag{7}$$

where

$$K=\left(\frac{1+\cos\beta}{16}\right)\left[\frac{2}{\pi}+\frac{\pi}{4}\left(1+\cos\beta\right)\cos\phi\right]^{1/2},$$

β is the contact angle of the heat transfer surface, and ϕ is the angle between the heat transfer surface and the horizontal plane. In general, for a heat transfer surface inclined at an angle f, it is 0° when horizontal and 90° when it is perpendicular to the surface.

The model is based on boiling heat transfer data received from heat transfer materials under various metals, with the contact angle data being replaced in the computation, a K value of about 0.107 is obtained. The CHF of each surface may now be calculated independently and normalized using the Kandlikar formula, *i.e.* $\mathrm{CHF}_{\mathrm{experimental}}/\mathrm{CHF}_{\mathrm{Kandlikar\ model}}$. Thermal mass is the product of specific heat and density, represented as a given substance must absorb per unit volume of heat when the temperature rises by one degree.

The specific data are listed in the following table.

Table 2. Boiling heat transfer data under different tested materials.

Material	Thermal conductivity (W/m·K)	Thermal mass (10^3 kJ/m^3·K)	Contact angle (°)	$\mathrm{CHF}_{\mathrm{experimental}}$	$\mathrm{CHF}_{\mathrm{Kandlikar\ model}}$	$\mathrm{CHF}_{\mathrm{experimental}}/\mathrm{CHF}_{\mathrm{Kandlikar\ model}}$
Brass	109	3.23	71	50.1	89.8	0.558
Aluminum	201	2.4	72	78.1	89.8	0.870
Copper	398	3.4	71	87.6	89.8	0.976

The variation of the normalized CHF is evaluated against a range of parameters, as shown in Table 2. The internal parameters of the test section, such as thermal conductivity, thermal diffusivity, and thermal effusivity, are connected to the measured CHFs to explain CHF discrepancy. Thermal diffusivity ($k/\rho c_{\mathrm{p}}$) is defined as the ratio of thermal conductivity to thermal mass,[42] whereas thermal effusivity ($\sqrt{k\rho c_{\mathrm{p}}}$) characterizes the ability to exchange thermal energy with its surroundings.[43] Table 2 shows that the trajectory of thermal conductivity is similar to the trend of normalized CHF ratio. As a consequence, the combination parameter of thermal conductivity and ρc_{p} is considered, and the linearly fitted k, $k/\rho c_{\mathrm{p}}$, $k\rho c_{\mathrm{p}}$, $\sqrt{k}$, $\sqrt{k/\rho c_{\mathrm{p}}}$, $\sqrt{k\rho c_{\mathrm{p}}}$, and normalized CHF value are analyzed respectively.

Figures 4(a)–4(f) depicts the normalized CHF of each test surface as a function of k, $k/\rho c_{\mathrm{p}}$, $k\rho c_{\mathrm{p}}$, $\sqrt{k}$, $\sqrt{k/\rho c_{\mathrm{p}}}$, and $\sqrt{k\rho c_{\mathrm{p}}}$. The functions of thermal conductivity and normalized CHF are shown in Figs. 4(a) and 4(d). The points in the graph are not linearly related, which shows that thermal conductivity is not a significant consideration in determining the CHF of the substrate. As shown in Figs. 4(b) and 4(e), the product of thermal conductivity and thermal mass does not have a strong association with the normalized CHF. The dots in the figure are random, and so is the product, proving the earlier conclusion that the normalized CHF value has little correlation with the product of ρ, c_{p}, and ρc_{p}. It is clear from Figs. 4(c) and 4(f) that $k/\rho c_{\mathrm{p}}$ has a linear relationship with the normalized CHF. To establish the correlation among these six sets of data, the data is linearly fitted and tested for the degree of relevance.

Figure 4 shows that the normalized CHF *versus* $k/\rho c_{\mathrm{p}}$, $\sqrt{k/\rho c_{\mathrm{p}}}$ provides the greatest match, with an R^2 value for a linear fit of 0.94 and 0.98, respectively. It indicates that there is a linear dependence between CHF and the parameter $k/\rho c_{\mathrm{p}}$, $\sqrt{k/\rho c_{\mathrm{p}}}$. A dimensionless correction factor is applied to the Kandlikar model to account for the effect of the substrate's physical parameters on predicting CHF. The inserted correction factor is the ratio of the substrate's characteristic value to the reference material's characteristic value. Copper is chosen

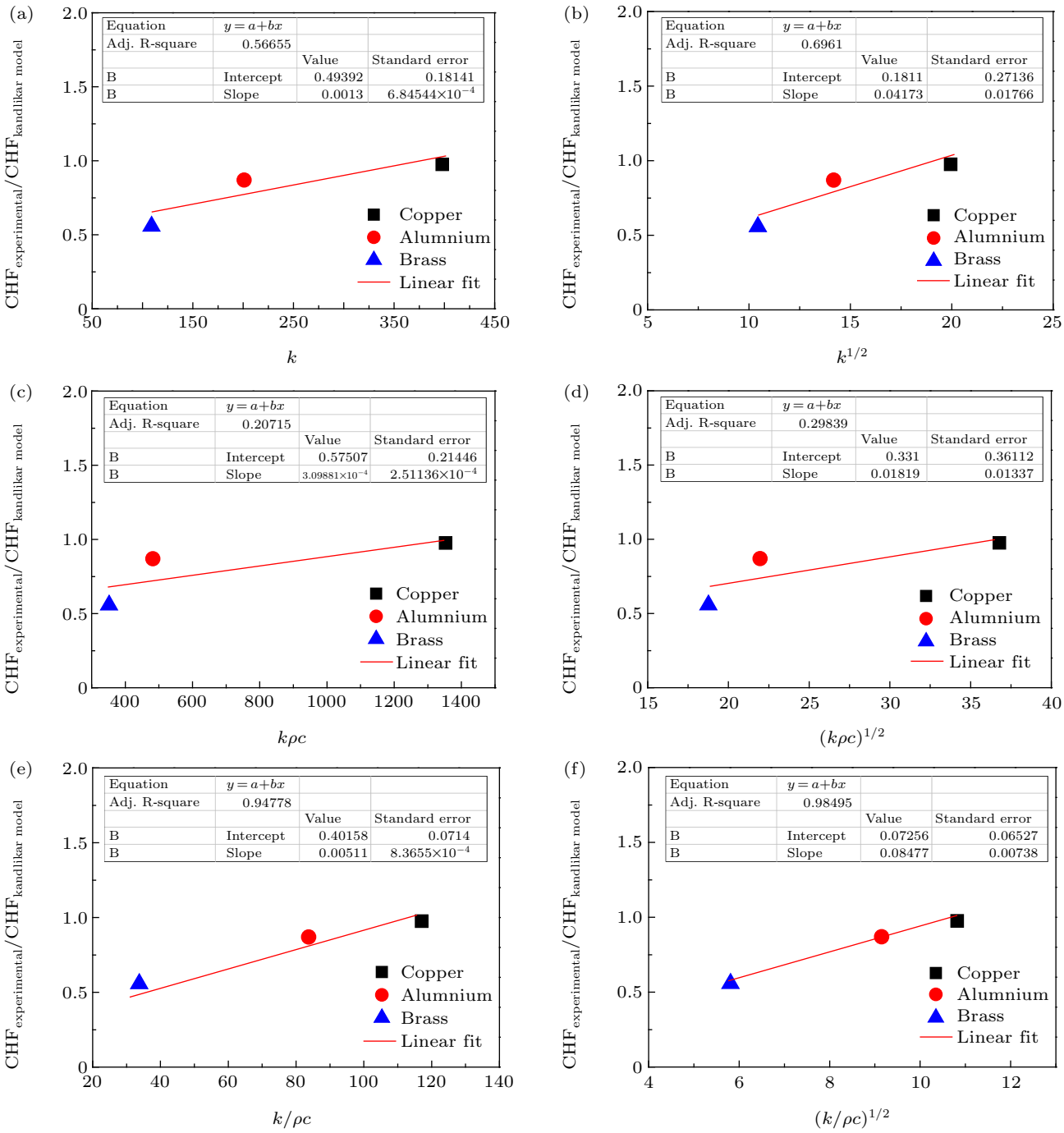


Fig. 4. The analyze of k, $k/\rho c_p$, $k\rho c_p$, $\sqrt{k}$, $\sqrt{k/\rho c_p}$, $\sqrt{k\rho c_p}$, and the normalized CHF value.

as the reference material for this study because its CHF has been widely reported in the literature and is almost identical to the CHF predicted by the Kandlikar model. The following is the equation derived by substituting:

$$q = \beta \times h_{fg}\rho_g^{1/2}\left(\frac{1+\cos\theta}{16}\right)\left[\frac{2}{\pi}+\frac{\pi}{4}(1+\cos\theta)\cos\varphi\right]^{1/2} \times [\sigma g(\rho_l-\rho_g)]^{1/4}, \quad (8)$$

where

$$\beta_1 = (k/\rho c)_{\text{material}} / (k/\rho c)_{\text{copper}}$$

or

$$\beta_2 = \left(\sqrt{k/\rho c}\right)_{\text{material}} / \left(\sqrt{k/\rho c}\right)_{\text{copper}}.$$

A comparison between the experimentally obtained CHF and the CHF predicted using the equation is shown in Fig. 5. The substrate material consists of three different heat transfer materials: brass, aluminum and copper with the calculated CHF of copper as the reference material value.

Figure 5(a) shows a comparison between the experiment and the prediction calculated using β_1 as the correction factor. The solid line indicates the value when $\text{CHF}_{\text{predicted}}/\text{CHF}_{\text{experimental}} = 1$, and the dotted line represents

the difference between the experimental and predicted CHF values. The dotted line for brass is at −50%, indicating a 50% difference between predicted and experimental CHF values, with a high inaccuracy that makes further forecasts unfeasible. Figure 5(b) shows the comparison diagram of the experiment and the prediction generated with a correction factor of β_2. All materials' CHF are properly predicted by the improved model, with an error of less than 5%. It can be observed that the predicted values are quite accurate for materials with high $k/\rho c_p$, such as copper, and the ratio essentially falls on the center of the solid line. The correction factor of high linear correlation considerably boosts the forecast for materials with low $k/\rho c_p$. Therefore, the correction factor is chosen to be β_2.

The Kandlikar model is further revised after considering the thermal properties of the heater material, based on the above-mentioned experimental simulation verification:

$$q = \beta \times h_{fg}\rho_g^{1/2}\left(\frac{1+\cos\theta}{16}\right)\left[\frac{2}{\pi}+\frac{\pi}{4}(1+\cos\theta)\cos\varphi\right]^{1/2} \times [\sigma g(\rho_l-\rho_g)]^{1/4}, \quad (9)$$

where $\beta = (\sqrt{k/\rho c})_{\text{material}}/(\sqrt{k/\rho c})_{\text{copper}}$.

The actual maximum error value is 4.8%, which is within the range of 5%.

Table 3 compares the CHF of different heater substrates in saturated pool boiling, which demonstrates that the predict CHF of heater substrates in our study is remarkable among the values. Besides, it can be seen clearly that the modified model predicts the CHF in this work is the most accurate with a minimum error value of 5%. Therefore, by extending the trends that have been reported in the literature[18,42,43] and appropriately choosing the heater thickness, it can be seen that the $\sqrt{k/\rho c}$ term proposed in the present work is able to account for the variation in CHF for the thick heaters that are beyond the asymptotic thickness. The thermal characteristics of the substrate give a more credible explanation for the CHF discrepancies observed. Consequently, it can be tentatively concluded that thermal properties of the heater substrates are primarily responsible for the CHF differences between the tested materials in the pool boiling condition.

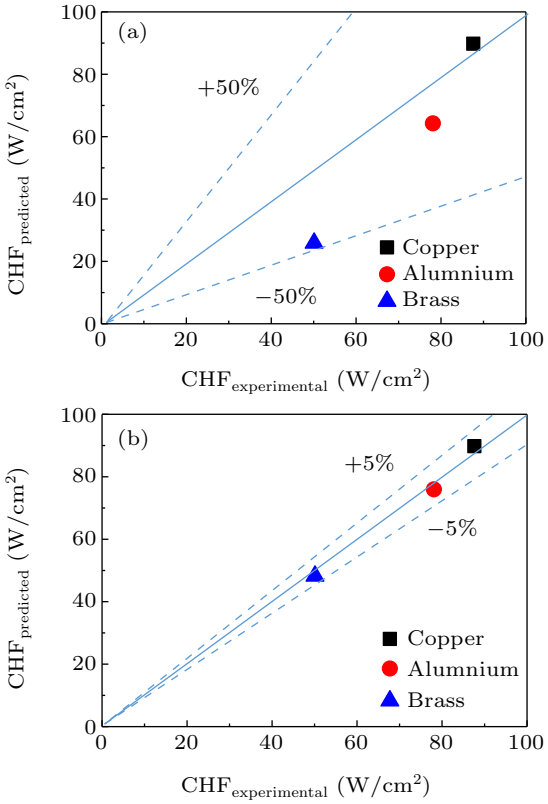


Fig. 5. Experimental *versus* predicted CHF; (a) a comparison between the experimental and the predicted CHF using β_1 as the correction factor; (b) a comparison between the experimental and the predicted CHF using β_2 as the correction factor.

Table 3. Comparison of heater substrates and error value in saturated pool boiling in literature.

Heater substrates	Working fluid	Nonhydrodynamic factor	Error value[a]	Reference
Cu, SS, and SA508	water	$\sqrt{\rho c_p k}$	15%	Ref. [19]
Aluminum, brass, copper, carbon steel, monel 400, silver, and silicon	water	$\sqrt{\rho c_p}$	15%	Ref. [36]
Inconel, SS, monel, Steel, iron, nickel, brass, aluminum, and coppr	FC-72	$\sqrt{\rho c_p k}$	8.4%	Ref. [17]
Silver, copper, zinc, nickel, and tin	water	$\sqrt{\rho c_p k}$	15%	Ref. [44]
Aluminum, coppr, and silicon	FC-72	$\frac{\delta\sqrt{\rho c_p k}}{\delta\sqrt{\rho c_p k}+0.1}$	12.5%	Ref. [24]
Aluminum, brass, and copper	water	$\sqrt{\frac{k}{\rho c_p}}$	5%	this work

[a]The error value is the modified model predicts of the CHF comparing with the experimental CHF data. δ is the thickness of the heater substrate.

4. Conclusion

In summary, the impacts of thermal characteristics are determined using detailed experimental findings from three different heaters operating at atmospheric pressure with water as the working fluid. To account for the variance of the heater's thermal characteristics, a non-dimensional substrate correction factor β is included. The CHF of thick heaters is found to be proportional to $\sqrt{k/\rho c}$, and the modified equation can accurately estimate the CHF of the surfaces tested within 5% error for aluminum, brass, and copper. This study shows new insight into the role of the heater substrate in enhancing CHF and provides an improved model for accurate

prediction of CHF values for advanced thermal management applications.

Acknowledgments

Project supported by the National Key Research and Development Program of China (Grant No. 2018YFA0702100), the National Natural Science Foundation of China (Grant No. U21A2079), the Zhejiang Provincial Key Research and Development Program of China (Grant Nos. 2021C05002 and 2021C01026), and the Fundamental Research Funds for the Central Universities.

References

[1] Pop E 2010 *Nano Res.* **3** 147
[2] Forrest E, Williamson E, Buongiorno J, Hu L, Rubner M and Cohen R 2010 *Int. J. Heat Mass Transfer* **53** 58
[3] Zhang W, Chai Y, Xu J, Liu G and Sun Y 2018 *Appl. Surf. Sci.* **457** 891
[4] Yu X, Xu J, Liu G and Ji X 2021 *Int. J. Heat Mass Transfer* **164** 120460
[5] Ji X, Xu J, Zhao Z and Yang W 2013 *Exp. Therm. Fluid Sci.* **48** 198
[6] Quan X, Dong L and Cheng P 2014 *Int. J. Heat Mass Transfer* **76** 452
[7] Rahman M M, Ölçeroğlu E and McCarthy M 2014 *Langmuir* **30** 11225
[8] Chu K, Enright R and Wang E N 2012 *Appl. Phys. Lett.* **100** 241603
[9] Rohsenow W M and Griffith P 1956 *Chem. Eng. Prog. Symp. Ser.* **18** 47
[10] Zuber N 1958 *Trans. ASME* **80** 711
[11] Haramura Y and Katto Y 1983 *Int. J. Heat Mass Transfer* **26** 389
[12] Yagov V V 2014 *Int. J. Heat Mass Transfer* **73** 265
[13] Theofanous T G, Dinh T N, Tu J P and Dinh A T 2002 *Exp. Therm. Fluid Sci.* **26** 793
[14] Mudawar I, Howard A H and Gersey C O 1997 *Int. J. Heat Mass Transfer* **40** 2327
[15] Zuber N 1959 *Atomic Energy Commission Report*
[16] Kandlikar S G 2001 *Journal of Heat Transfer* **123** 1071
[17] Golobič I and Bergles A E 1997 *Exp. Therm. Fluid Sci.* **15** 43
[18] Lee S K, Liu M, Brown N R, Terrani K A and Lee Y 2020 *Nucl. Technol.* **206** 339
[19] Mei Y, Shao Y, Gong S, Zhu Y and Gu H 2018 *Int. J. Heat Mass Transfer* **121** 632
[20] Jun S, Kim J, You S M and Kim H Y 2016 *Int. J. Heat Mass Transfer* **103** 277
[21] Rainey K N and You S M 2001 *Int. J. Heat Mass Transfer* **44** 2589
[22] Kim J S, Girard A, Jun S, Lee J and You S M 2018 *Int. J. Heat Mass Transfer* **118** 802
[23] Ferjancic K and Golobic I 2002 *Exp. Therm. Fluid* **25** 565
[24] Arik M and Bar-Cohen A 2003 *Int. J. Heat Mass Transfer* **46** 3755
[25] Tachibana F, Akiyama M and Kawamura H 1967 *J. Nucl. Sci. Technol.* **4** 121
[26] Westwater J W, Hwalek J J and Irving M E 1986 *Ind. Eng. Chem. Fundam* **25** 685
[27] Zhang S Y, Zhang X Z, Jin T, Tang K and Huang Y Z 2011 *Cryogenics* **4** 7
[28] Grigoriev V A, Klimenko V V, Pavlov Y M and Ametistov E V 1978 *The influence of some heating surface properties on the critical heat flux in cryogenic liquids boiling* (Begel House Inc.)
[29] Cooke D and Kandlikar S G 2012 *Int. J. Heat Mass Transfer* **55** 1004
[30] Jaikumar A and Kandlikar S G 2015 *Int. J. Heat Mass Transfer* **88** 652
[31] Patil C M, Santhanam K S V and Kandlikar S G 2014 *Int. J. Heat Mass Transfer* **79** 989
[32] Hong S, Jiang S, Hu Y, Dang C and Wang S 2019 *Int. J. Heat Mass Transfer* **136** 235
[33] Kim J S, Girard A, Jun S, Lee J and You S M 2018 *Int. J. Heat Mass Transfer* **118** 802
[34] Singh A, Mikic B B and Rohsenow W M 1976 *ASME J. Heat Transfer* **98** 401
[35] Pioro I L, Rohsenow W and Doerffer S S 2004 *Int. J. Heat Mass Transfer* **47** 5033
[36] Raghupathi P A and Kandlikar S G 2017 *Journal of Heat Transfer* **139** 111502
[37] Lim D Y and Bang I C 2020 *Int. J. Heat Mass Transfer* **150** 119360
[38] M J and W F 1931 *Forschung auf dem Gebiete des Ingenieurwesens* **2** 435
[39] Kutateladze S S and Schneiderman L L 1953 *USAEC Report*, AECtr **3405** 95
[40] Kutateladze S S 1951 *Izv. Akad. Nauk SSSR, Otd. Tech. Nauk* **4** 529
[41] Kutateladze S S 1948 *Kotloturbostroenie* **3** 10
[42] Lee S K, Liu M, Brown N R, Terrani K A, Blandford E D, Ban H, Jensen C B and Lee Y 2019 *Int. J. Heat Mass Transfer* **132** 643
[43] Mei Y, Shao Y, Gong S, Zhu Y and Gu H 2018 *Int. J. Heat Mass Transfer* **121** 632
[44] Magrini U and Nannei E 1975 *J. Heat Transfer* **97** 173